Internet-based Real-time Obstacle Avoidance of a Mobile Robot

Jae-Pyung Ko, Jang-Myung Lee*
Department of Electronics Engineering, Pusan National University, Pusan 609-735, Korea

In this research, a remote control system has been developed and implemented, which combines autonomous obstacle avoidance in real-time with force-reflective tele-operation. A tele-operated mobile robot is controlled by a local two-degrees-of-freedom force-reflective joystick that a human operator holds while he is monitoring the screen. In the system, the force-reflective joystick transforms the relation between a mobile robot and the environment to the operator as a virtual force which is generated in the form of a new collision vector and reflected to the operator. This reflected force makes the tele-operation of a mobile robot safe from collision in an uncertain and obstacle-cluttered remote environment. A mobile robot controlled by a local operator usually takes pictures of remote environments and sends the images back to the operator over the Internet. Because of limitations of communication bandwidth and the narrow view-angles of the camera, the operator cannot observe shadow regions and curved spaces frequently. To overcome this problem, a new form of virtual force is generated along the collision vector according to both distance and approaching velocity between an obstacle and the mobile robot, which is obtained from ultrasonic sensors. This virtual force is transferred back to the two-degrees-of-freedom master joystick over the Internet to enable a human operator to feel the geometrical relation between the mobile robot and the obstacle. It is demonstrated by experiments that this haptic reflection improves the performance of a tele-operated mobile robot significantly.

Key Words : Tele-operation, Collision Vector, Force Reflection, Virtual Impedance, Obstacle Avoidance

1. Introduction

The conventional tele-operation of mobile robots rely on visual contact with the operator, either directly or through video transmissions. Under such conditions, a human tele-operator must exercise extreme care, especially in obstacle-cluttered environments. Consequently, the actual traveling speed of the mobile robot might be very slow. When dust, smoke, or steam inhibits vision based guidance, conventional tele-operated activity is ruled out altogether. Teleautonomous system, which is explained in the previous study (Borenstein and Koren, 1990) can overcome this problem, that combines autonomous obstacle avoidance with tele-operation. In this system, the tele-operator can guide the mobile robot even without any visual contact. The mobile robot follows the general direction prescribed by the operator. When the robot encounters an obstacle, it autonomously avoids collision with that obstacle, trying to match the operator's prescribed direction as close as possible.

Telepresence is the ultimate factor in reliable and skillful tele-operations. If all the information

* Corresponding Author,
E-mail : jmlee@pusan.ac.kr
TEL : +82-51-510-2378; **FAX** : +82-51-515-5190
Department of Electronics Engineering, Pusan National University, Pusan 609-735, Korea. (Manuscript **Received** December 27, 2004; **Revised** May 4, 2005)

at a remote site can be transferred to a human operator in real time, telepresence can be achieved naturally. In a reliable tele-operation system, bilateral control, in which information at the remote and operator sites is shared together, is generally utilized. In most cases of bilateral tele-operations, position information is reflected to the operator as images while the operator is holding a joystick for the generation of motion commands. However, this visual information is not always sufficient. For example, when a mobile robot enters a tunnel, the capturing of environmental images is delayed for a few seconds.

As explained in the previous studies (Kim et al., 1992; Lawrence, 1993; Lee and Lee, 2000; Elhajj et al., 2001), one of the general trends in reliable tele-operation is to generate a virtual force between a robot and the environment, which, in addition to the visual information, is transferred to a human operator through a joystick as tactile information (Lee and Lee, 2000). Among the studies of tele-operated mobile robots which seriously investigate collisions between mobile robots and obstacles, there are not many studies that focus on bilateral control using force reflection (Elhajj et al., 2001).

In this paper, we have developed a system that combines autonomous obstacle avoidance with force reflective tele-operation. In this system, a tele-operated mobile robot is controlled by a local two-degrees-of- freedom force-reflective joystick that a human operator holds while he is monitoring the screen. The force-reflective joystick transforms the relation between a mobile robot and the environment to the operator as a virtual force. As shown in Figure 1, a bilateral tele operation system consists of an operator, a joystick, a communication block, and a mobile robot. The virtual force from a mobile robot, which is a function of the distance and relative velocity between a mobile robot and an obstacle, is reflected to the joystick as a force between the joystick and the human hand using two motors in the joystick. Therefore, the operator can feel, and avoid, collisions through the haptic joystick in spite of the limitations in visual display, which are transmission delay, limited bandwidth, bad

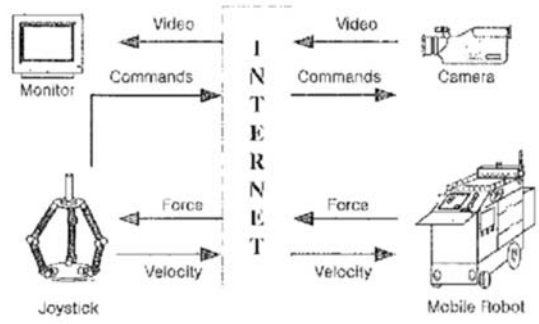

Fig. 1 Block diagram of the tele-operation system

illumination, occulusion, and camera distortions.

To generate the virtual force, the relation between a mobile robot and an obstacle, and to guide autonomous operation of mobile robot is modeled as a virtual mass-spring-damper, that is, an impedance. The virtual impedance method considering the approach velocity to an obstacle seems to be more suitable than the conventional potential field methods, since it has the capability to cope with moving obstacles. However, the obstacle avoidance strategy should be properly modified for the different shapes of the obstacles. As a major contribution of this study, a collision vector is newly defined from the ultrasonic sensor data, which is normal to the obstacle. Through the experiments, the effectiveness of the collision vector in avoiding local minima is demonstrated.

2. System Model

A bilateral tele-operation system is composed of a human operator, a joystick, a Global Path Planner (GPP), a remote PC, a mobile robot and a communication block, as shown in Figure 2. If a human operator exerts force F_h to the joystick, the displacement of the joystick is generated as X_m. Based on the data, the GPP generates the optimal trajectory for the mobile robot to the goal, and transfers the data to a Dynamic Avoidance Planner (DAP) that makes the robot follow the given trajectory while avoiding the obstacles. That is, the GPP (local PC) creates X_d and V_d according to the X_m, and transfers them to the remote PC through the Internet. When the slave mobile robot receives X_d and V_d from the remote

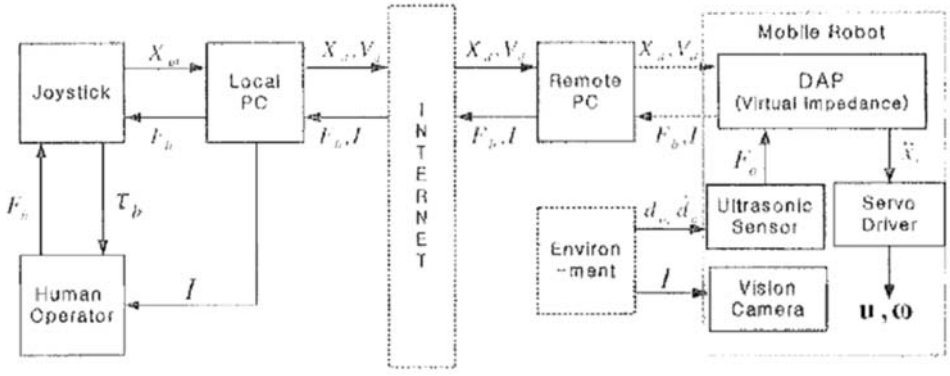

Fig. 2 Tele-operation system architecture

PC through a wireless LAN, the DAP of the mobile robot generates $\ddot{x}_s$ according to X_d, V_d, and the data from ultrasonic sensors. Then, $\ddot{x}_s$ is transferred to the servo-driver that generates **u** and ω (the control inputs of a mobile robot) to track the given path.

With this system architecture, the operator at the local site can feel the telepresence by means of the feedback data that are composed of the repulsive force F_b, between the mobile robot and obstacles, and the visual information, I.

2.1 Master (Joystick) system model

A human operator can feel the virtual force generated between a tele-operated mobile robot and the remote environment through the two-degrees-of-freedom joystick as shown in Figure 3.

Figure 4 shows the block diagram of a joystick system. To control the joystick, which basically generates motion commands, a joystick controller was designed using an 80C196KC microprocessor. This joystick also retrieves the force data F_b that is sent from the remote PC to the operator. For this retrieval, two axial motors are driven by PWM (Pulse Width Modulation) outputs corresponding to the F_b. L298N DC motor drives are used to amplify the power. The position of the joystick is measured by potentiometers connected to each axis. An A/D (Analog to Digital) converter transforms the voltage measured by the potentiometers into 10-bit digital data that are reflected to the joystick controller as inputs. To measure the force at the joystick held by an

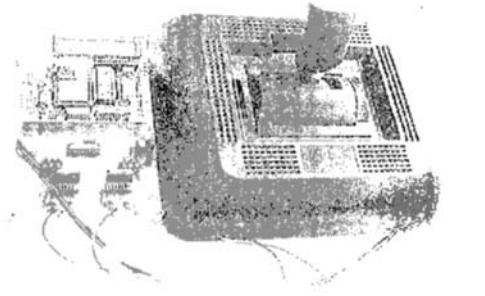

Fig. 3 2 DOF joystick system

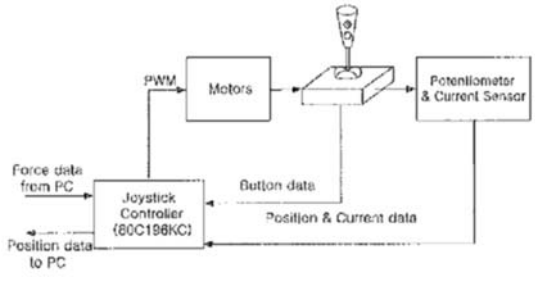

Fig. 4 Block diagram of a joystick system

operator, a current sensor is used. The current through the sensor is transformed into voltage by a 2 Ω resister and passed through an LPF (Low Pass Filter). The resultant voltage is converted into 10-bit digital data by the A/D converter. The digital data are also delivered to the joystick controller as control inputs.

2.1.1 Human operator's commands

When the operator exerts force F_h to the joy-

stick, this force F_h creates the joystick displacement X_m. When the x-axis is aligned to the heading of the mobile robot, X_m generates the desired velocity V_d and the desired position X_d of the robot as follows:

$$V_d(t)=K_m\cdot X_m(t) \tag{1}$$

$$X_d(t)=\int_0^{T_3} K_v\cdot V_d(t)\cdot dt \tag{2}$$

where $X_m=\begin{bmatrix}X_{mx}\\X_{my}\end{bmatrix}$, $X_d=\begin{bmatrix}X_{dx}\\X_{dy}\end{bmatrix}$, $V=\begin{bmatrix}V_{dx}\\V_{dy}\end{bmatrix}$, K_m and K_v are scaling constants, and T_3 is the sampling time for the GPP.

2.1.2 Virtual force feedback

The virtual force F_b reflected to the operator is represented as

$$F_b=\sum_{i=1}^{n} F_{oi}(t) \tag{3}$$

where n is the number of obstacles.

The F_b which is generated from a mobile robot at a remote site, is transferred to the operator at the master site as

$$\tau_b(t)=sat(K_b\cdot F_b(t)) \tag{4}$$

$$sat(x)=\begin{cases}x & \text{, if } |x|\le x_{\max}\\ sign(x)\cdot x_{\max} & \text{, otherwise}\end{cases} \tag{5}$$

where K_b is the force feedback gain constant. And the saturation function, $sat(x)$, is used so as to prevent the feedback force F_b from exceeding the driving power of the motor.

In spite of the limited information from the visual feedback such as the transmission delay of a channel, the limitation of bandwidth, and the camera distortion, now the operator can recognize the geometrical relation between the robot and the objects realistically with the aid of the force τ_b felt from the joystick.

2.2 Slave (Mobile Robot) model

Figure 5 shows the configuration of the mobile robot used for this research. In the middle of the mobile robot, the sixteen ultrasonic sensors are attached at every 22.5° to acquire the distance data to the obstacles. And vision sensor (camera), gyro sensor, electric compass sensor module, encoder sensors and collision perception sensors are attached to improve autonomous mobility of the mobile robot. The whole system is composed of a master and four slave control module as shown in Figure 6. The tasks are decentralized in each control module, which is able to handle real-time multi-sensor data processing and control of mobile robot. The master and four slave control module can communicate through CAN line.

Fig. 5 The configuration of the mobile robot

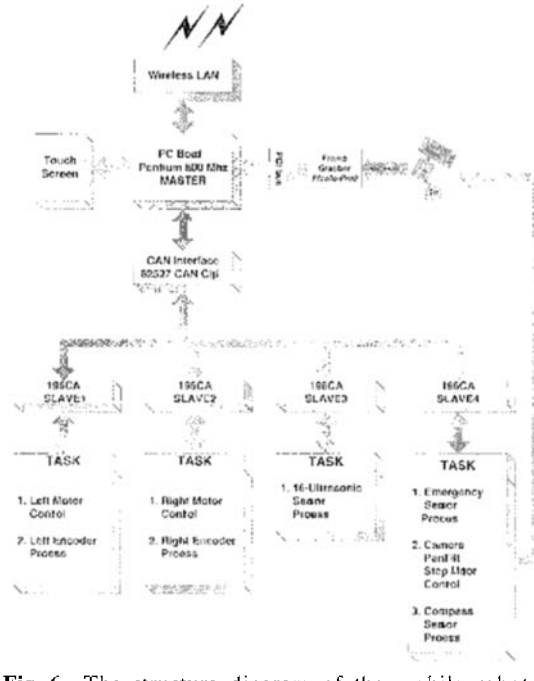

Fig. 6 The structure diagram of the mobile robot system

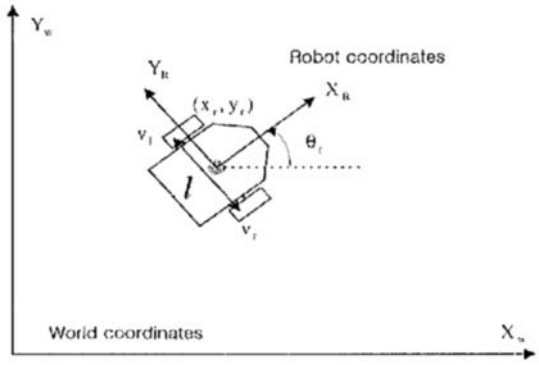

Fig. 7 A mobile robot model

The state of mobile robot is represented as a vector $\mathbf{p}=[x\ y\ \theta]^T$ composed of position and orientation variables as shown in Figure 7. In general, the motion of the mobile robot can be modeled by the translation velocity, **u**, and the angular velocity, ω (Zhao and BeMent, 1992; Roh et al., 2001). The translation velocity, **u**, and angular velocity, ω are calculated using each encoder data of wheel and gyro sensor at each control period.

$$u=\frac{1}{2}(v_R+v_L) \tag{6}$$

$$\omega=\frac{1}{l}(v_R-v_L) \tag{7}$$

The velocity of mobile robot in the world coordinates is represented as a Jacobian matrix $J(p)$ according to input variable q. And position and orientation vector **p** is represented as an integral equation.

$$\dot{\mathbf{p}}=J(p)\,\dot{\mathbf{q}}$$

$$\begin{bmatrix}\dot{x}\\ \dot{y}\\ \dot{\theta}\end{bmatrix}=\begin{bmatrix}\cos\theta & 0\\ \sin\theta & 0\\ 0 & 1\end{bmatrix}\begin{bmatrix}u\\ \omega\end{bmatrix} \tag{8}$$

$$\mathbf{p}=\begin{bmatrix}x\\ y\\ \theta\end{bmatrix}=\begin{bmatrix}x_0\\ y_0\\ \theta_0\end{bmatrix}+\begin{bmatrix}\int u(\tau)\cos(\theta(\tau))\,d\tau\\ \int u(\tau)\sin(\theta(\tau))\,d\tau\\ \int \omega(\tau)\,d\tau\end{bmatrix} \tag{9}$$

2.2.1 Reference trajectory generation

A remote mobile robot implements the obstacle avoidance in real time according to the reference trajectory created by an operator. As illustrated in Figure 8, $V_d(t)$ and $X_d(t)$ from the master are transformed into the robot coordinates and represented as $\dot{X}_r(t)$ and $X_r(t)$ which are

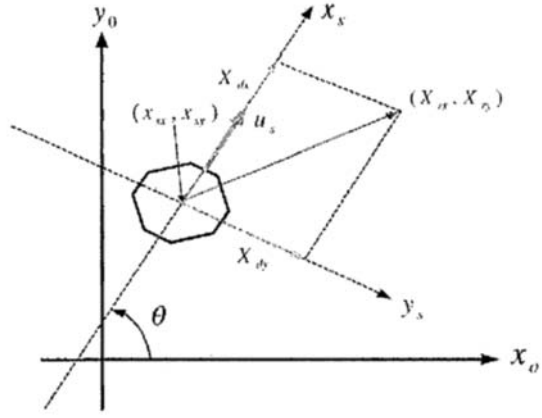

Fig. 8 Generation of reference trajectory

$$\begin{bmatrix}\dot{X}_{rx}(x)\\ \dot{X}_{ry}(t)\end{bmatrix}=\begin{bmatrix}\cos\theta & -\sin\theta\\ \sin\theta & \cos\theta\end{bmatrix}\begin{bmatrix}V_{dx}(t)\\ V_{dy}(t)\end{bmatrix} \tag{10}$$

and

$$\begin{bmatrix}X_{rx}(t)\\ X_{ry}(t)\\ 1\end{bmatrix}=\begin{bmatrix}\cos\theta & -\sin\theta & x_{sx}(t)\\ \sin\theta & \cos\theta & x_{sy}(t)\\ 0 & 0 & 1\end{bmatrix}\begin{bmatrix}X_{dx}(t)\\ X_{dy}(t)\\ 1\end{bmatrix} \tag{11}$$

where (x_{sx}, x_{sy}) represents the current robot coordinates.

3. A New Virtual Impedance Algorithm

As shown in Figure 9, in the GPP, the human operator generates $X(t)$ and $\dot{X}(t)$ using

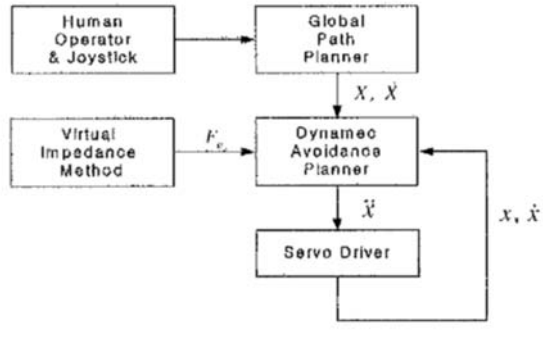

Fig. 9 Trajectory tracking and obstacle avoidance

the joystick, while in the DAP, the command to the servo driver, $\dot{x}(t)$, is generated to track the given trajectory $X(t)$, $\dot{X}(t)$, as well as to avoid obstacles based on the virtual impedance model. Before proposing a new virtual impedance algorithm, the related work is surveyed in order to provide a firm basis for this research.

3.1 Review of obstacle avoidance method

Approaches to obstacle avoidance are reviewed and discussed in view of their applicability to real-time obstacle avoidance.

3.1.1 Edge detection methods

A general and commonly employed method is based on edge-detection (Borenstein and Koren, 1988). In this method, the algorithm tries to determine the vertical edges of the obstacle and consequently attempts to steer the robot around an edge. The line connecting the two edges is considered to represent one of the obstacle's boundaries. A disadvantage of the obstacle avoidance method based on the edge detection is that the robot needs to stop in front of the obstacle. Therefore it is not suitable for real-time obstacle avoidance.

3.1.2 Certainty grid methods

In the certainty grid world model (Elfes, 1987), the robot's work area is represented by a two-dimensional array of square elements denoted as cells. Each cell contains a CV (certainty value) that indicates the measure of confidence that an obstacle exists within the cell area. This method is not suitable for the real-time obstacle avoidance, since it requires a robot to stop in order to scan the work area, and also because it has a heavy computational load.

3.1.3 Potential field method

Potential Field Method (Khatib, 1986; Borenstein and Koren, 1989) achieves the collision avoidance motion planning of a robot by generating a virtual force against obstacles and toward the goal. That is, it generates an attractive force between the mobile robot and a target and generates a repulsive force against an obstacle that the mobile robot confronts in navigation. This method has the advantage of making the fast motion planning for nearby obstacles, but has a shortcoming of getting into a local minimum where the attractive and the repulsive forces are equal. To overcome this local minimum problem, the extended virtual force field method (Borenstein and Koren, 1989) is proposed, where a free vector is added to the repulsive force. However the virtual force becomes larger for larger obstacles since the repulsive forces are coming from all obstacle-detecting sensors, which makes this method unsuitable for certain applications.

3.1.4 Virtual impedance method

Impedance control is an algorithm that adjusts the relation between a velocity command and contact force, which models the interconnection between an uncertain environment and a robot as impedance (Hogan, 1985). In the virtual impedance method (Arai et al., 1989; Ota et al., 1995), the impedance is used to generate a repulsive force for the navigation of a mobile robot in avoiding collisions with obstacles. As shown in Figure 10, the virtual impedance method generates a virtual force according to the distance and relative velocity between the robot and an obstacle, which can be modeled as a spring and a damper. Repulsive force F_o consists of repulsive forces against a static obstacle, F_{os}, and a dynamic obstacle, F_{od}. Obstacle avoidance is handled generally in the DAP, while the GPP generates the trajectory $X(t)$, $\dot{X}(t)$ according to the joystick output, X_m.

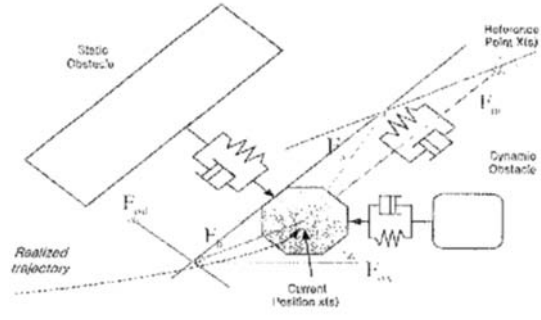

Fig. 10 Virtual impedance model

Virtual impedance can be defined as the following procedures. First of all, the acceleration for the mobile robot can be represented as

$$\ddot{x}_s = \frac{1}{M_s}\left\{F_m + \sum_{i=0}^{n} F_{oi}\right\} \tag{12}$$

where F_m is the attractive force generated between the current position of the robot and the reference point generated by the master, and F_{oi} is the virtual repulsive force between the current robot and a nearly i^{th} obstacle among n objects. Note that the virtual mass M_s does not represent the real "mass" of the robot but the relative rigidity of the robot trajectory.

The attractive force, F_m, is generated as

$$\begin{aligned} F_m &= K_r(X_{rs}) + D_r(\dot{X}_{rs}) \\ &= -K_r(x_s - X_r) - D_r(\dot{x}_s - \dot{X}_r) \end{aligned} \tag{13}$$

where x_s is the present position of the robot, and X_r is the reference point of the robot at the present time (planned by the GPP). And X_r and D_r are a spring and a damper constant between the robot and the reference point, respectively.

The summation of virtual repulsive force can be expressed as

$$\begin{aligned} F_o &= K_o(X_{so}) + D_o(\dot{X}_{so}) \\ &= \sum_{i=0}^{n}\{K_o(x_s - x_{oi}) + D_o(\dot{x}_s - \dot{x}_{oi})\} \end{aligned} \tag{14}$$

where K_o and D_o are a spring and a damper

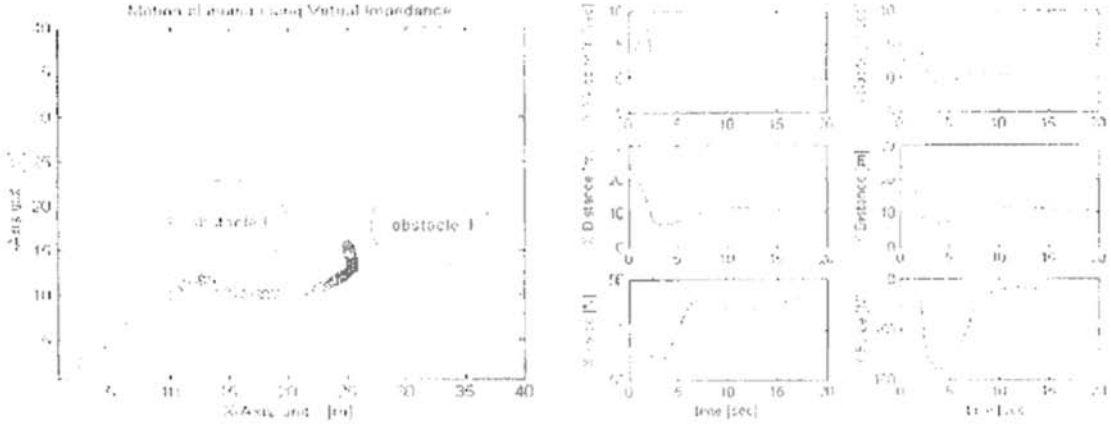

(a) A conventional virtual impedance method

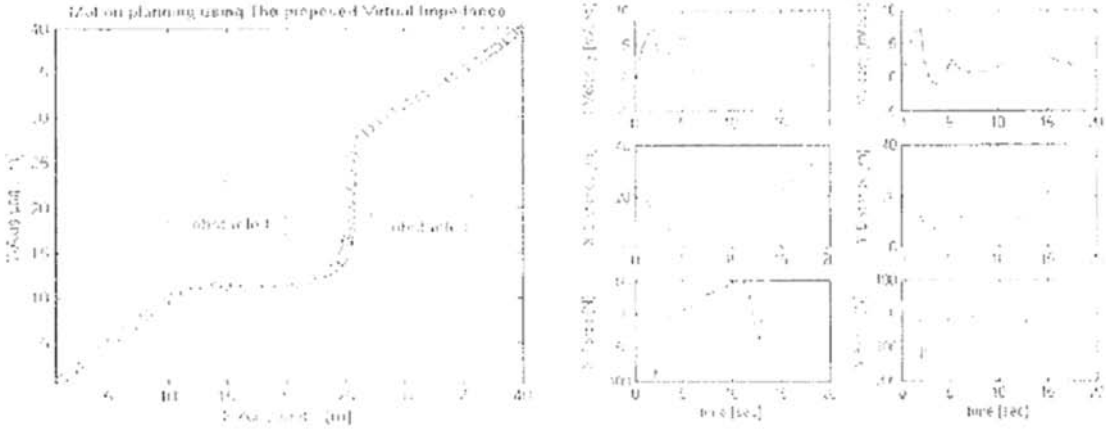

(b) A new virtual impedance method

Fig. 11 Simulation results of motion planning in case of a static obstacle (where K_r=2, D_r=10, K_o=15, D_o=15, and M_s=10)

constant between the robot and the obstacle, respectively, and x_{oi} and $\dot{x}_{oi}$ are the position and the velocity of the i^{th} obstacle, respectively. And n is the number of obstacles within the sensing area of the robot.

Actually, the feedback force F_b between the human hand and the joystick, which is physically the same as F_o, is maintained as a constant unless the operator moves the joystick to change the trajectory.

3.2 A new virtual impedance method

The virtual impedance method considering the approach velocity to an obstacle seems to be more suitable than the conventional potential field methods, since it has the capability to cope with moving obstacles. However, the obstacle avoidance strategy should be properly modified for the different shapes of the obstacles. For example, when the relative velocity between a mobile robot and an obstacle generates a repulsive force, the mobile robot cannot even approach near to the narrow channel, which is shown by the simulation in Figure 11(a). Going of obstacle and collision danger the mobile robot decreases moving velocity, then can succeed in collision avoidance by damper of big value. However, it represents a large-time delay or time slack is happened that stops in obstacle surroundings by damper's effect.

In this paper, therefore, we propose a new virtual impedance method that sets a damper as

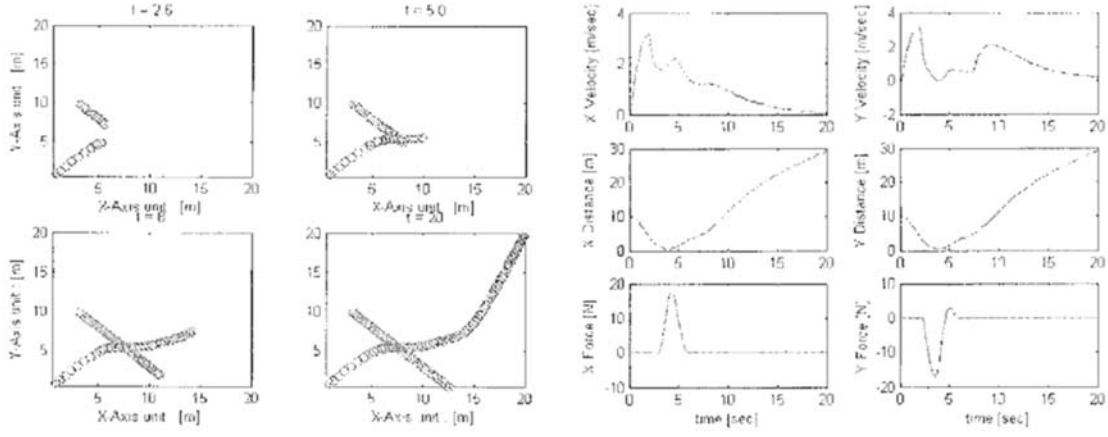

(a) A conventional virtual impedance method

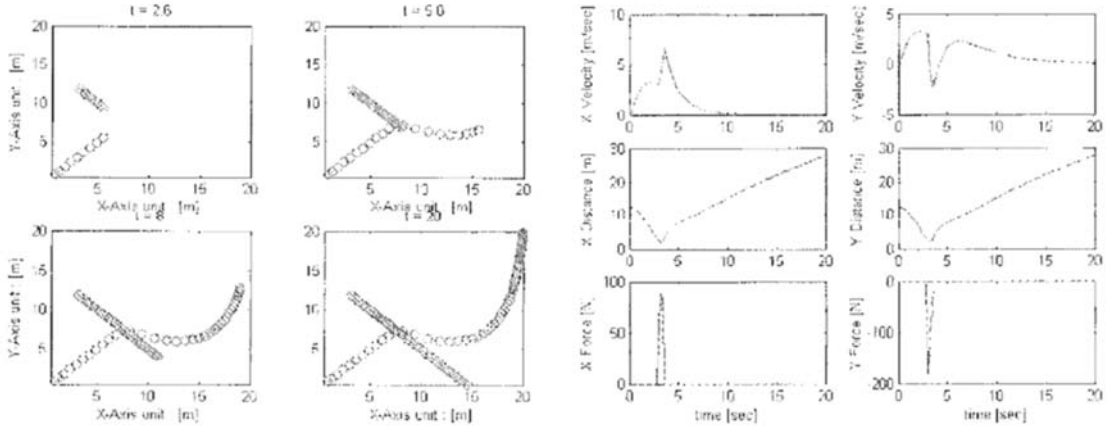

(b) A new virtual impedance method

Fig. 12 Simulation results of motion planning in case of a moving obstacle (where K_r=2, D_r=10, K_o=15, D_o=15, and M_s=10)

the rate change of the shortest distance between a mobile robot and an obstacle. The new proposed virtual impedance model is defined as

$$F_o(s)=K_o(X_{g,o}(s))+D_o(\dot{X}_{g,o}(s)) = \begin{cases} \sum_{i=0}^{n}\left\{K_o(\rho_0-\|d_i\|)\frac{d}{\|d_i\|}-D_o(\Delta(d_i))\frac{\dot{d}_i}{|\dot{d}_i|}\right\}, & \text{when } \|d_i\|<\rho_0 \\ 0, & \text{otherwise} \end{cases} \quad (15)$$

where d_i is the shortest vector to the obstacle, $\Delta(d_i)=d_i[t]-d_i[t-1]$, and ρ_o is the measurable range of an ultrasonic sensor and the simulation result is shown in Figure 11(b). The simulation result represents the mobile robot can succeed in collision avoidance and reach the goal with new virtual impedance method in case of using same parameters and $\rho_o \leq 13$.

Figure 12(a) and (b) show the simulation result of motion planning with virtual impedance method with both a conventional and a new virtual impedance method in case of a moving obstacle and the same parameters shown in Figure 11.

3.2.1 Detection of a collision vector for an obstacle

The shortest vector to the obstacle is renamed as a collision vector that can be obtained practically using the ultrasonic sensors. That is, we are going to define a normal vector to the tangential line of an obstacle as a collision vector. In the experimental robot, there are sixteen 6500-series ultrasonic sensors from Polaroid Company, to acquire the distance data between a mobile robot and obstacles. In real experiments, we cannot obtain accurate distance data in cases where the angle between a normal vector to a tangential line of an object and the beam of an ultrasonic sensor is more than 30 degrees. This is caused by poor directionality, specular reflections and frequent mis-readings of ultrasonic sensors, and limits the effective number of sensors for the collision vector decision to three, since there is an ultrasonic sensor every 22.5 degrees.

To generate the virtual repulsive force to avoid an obstacle that might be invisible, the collision vector for the obstacle needs to be obtained by using the ultrasonic sensors. Supposing that a mobile robot is moving in a building, the shape of obstacles can be classified as a cylinder (including a person) or a plane (a wall, a corner, etc). Therefore, with the ultrasonic sensors arranged in a circular pattern every 22.5 degrees, three cases of collision vectors shown in Figure 13 may

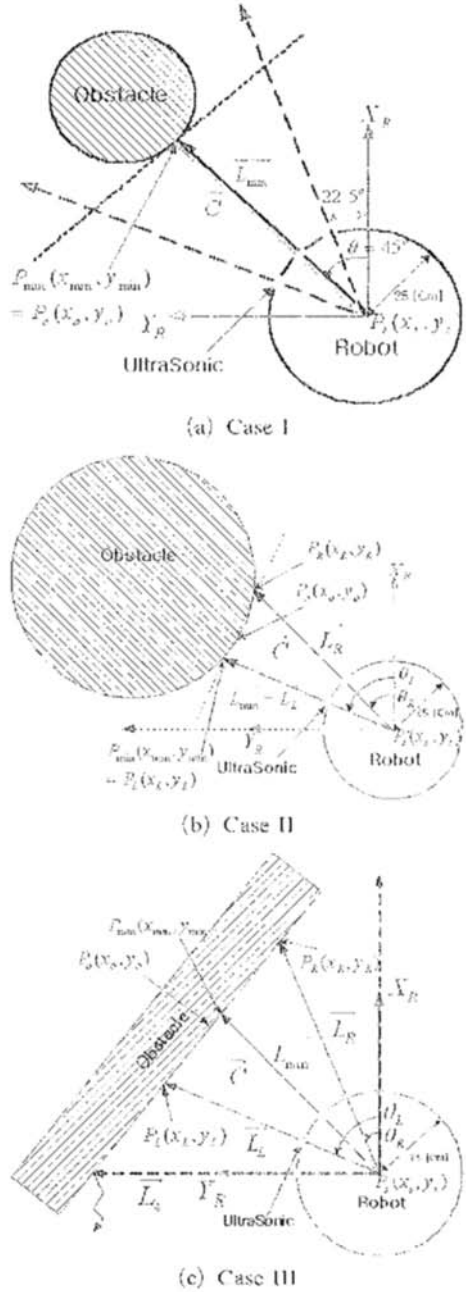

(a) Case I

(b) Case II

(c) Case III

Fig. 13 Collision vector against an obstacle

include all the possibilities of the relation between the robot and the obstacle.

Case I A small cylindrical obstacle which could be a person is detected by only one ultrasonic sensor. In this case, the collision vector, $\vec{C}$, can be obtained directly by

$$\vec{C} = -\vec{L}_{\min} \tag{16}$$

Case II An obstacle is detected by two neighboring ultrasonic sensors. In this case, first of all, we define the shorter distance vector as $\vec{L}_{\min}$. The other distance vector is defined as $\vec{L}_R$ in the case that it is to the right of $\vec{L}_{\min}$. Using the points P_L, P_R, the lines $\vec{L}_L$, $\vec{L}_R$, and the tangential line of the obstacle, $\overline{P_L P_R}$, can be obtained. And the normal vector to this line across the point P_s, that is, the collision vector, $\vec{C}\,(=\overrightarrow{P_o P_s})$, can be calculated to obtain the point P_o as

$$\vec{C} = \overrightarrow{P_o P_s} \tag{17}$$

$$P_o = (x_o, y_o) = \left(\frac{V \cdot x_L - y_L}{V + \frac{1}{V}}, -\frac{-x_L + \frac{1}{V} y_L}{V + \frac{1}{V}} \right) \tag{18}$$

where $V = \dfrac{y_L - y_R}{x_L - x_R}$.

Case III An obstacle is detected by three neighboring ultrasonic sensors. At first, the shortest distance vector among the three detected distance vectors is defined as $\vec{L}_{\min}$. Then, by the same procedure as in Case II, $\vec{C}$ can be calculated by Equation (17) and (18). Note that $\vec{L}_e$ is an unreliable datum, because the angle between $\vec{L}_e$ and $\vec{C}$ is over 30 degrees. Therefore, the collision vector, $\vec{C}$, can be obtained using only three distance vectors, $\vec{L}_{\min}$, $\vec{L}_L$ and $\vec{L}_R$.

Using $\vec{C}$, acquired above, the virtual impedance model proposed in Equation (15) can be modified according to

$$\begin{aligned} F_o(s) &= K_o(X_{s,o}(s)) + D_o(\dot{X}_{s,o}(s)) \\ &= \begin{cases} \sum_{i=1}^{n} \left\{ K_{s,o}(\rho_0 - \|\vec{C}\|)\, \vec{C}_{unit} - D_{s,o}(\Delta(\|\vec{C}\|))\, \vec{C}_{unit} \right\}, & \text{when } \|d_i\| < \rho_0 \\ 0 & \text{, otherwise} \end{cases} \end{aligned} \tag{19}$$

4. Simulations and Experimentation

4.1 Simulations

First of all, the effectiveness of a collision vector in obstacle avoidance is demonstrated through simulations. Figure 11(a) is the simulation result using the conventional virtual impedance model defined in Equation (14). Each small circle represents the location of the mobile robot at the k^{th} instance. The mobile robot is programmed to move from the left-bottom corner to the right-top goal while avoiding two obstacles in the middle of the reference trajectory. A large time delay or time slack is caused by the defined damper around obstacles, and the mobile robot is finally blocked at the center of two nearby obstacles. Figure 11(b) is a simulation result of the proposed impedance model defined in Equation (15). The damper causes the deceleration of the mobile robot before a collision and prevents the mobile robot from deviating from the programmed path after obstacle avoidance. Note that in the middle of the two obstacles, two collision vectors are generated, which become the bases for the repulsive forces mostly cancelled out by each other. At that moment, the attraction force to the goal plays the major role in guiding the mobile robot.

Note that in the tele-operation of a mobile robot with the conventional virtual impedance method, the robot may collide with a human in a corridor due to a large repulsive force for avoiding a wide wall, which becomes very large since all the repulsive forces from the wall-detecting sensors are combined. However, in this new scheme, the repulsive force from the nearby human is bigger than that from the wall since only a collision vector generates the repulsive force for each obstacle.

Now further simulations are performed to verify the superiority of this new virtual impedance-based obstacle avoidance scheme to the PFM. Figure 14(a) shows the case in which the virtual repulsive force becomes large for a wide wall according to the conventional PFM, while (b) shows the case in which the virtual repulsive force

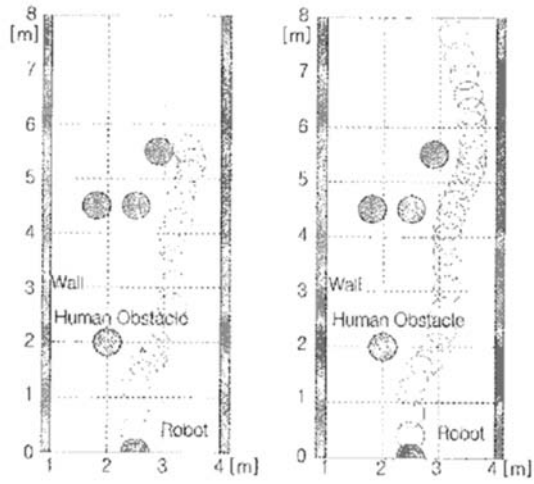

(a) Conventional PFM (b) Proposed collision vector method

Fig. 14 Comparison of the PFM and the proposed method

is generated by a collision vector for obstacle avoidance. Through a comparison of these two cases, the following can be concluded. In case (a), there is an oscillation of the mobile robot around point A. It is caused by the change of the sensor that detects the obstacle, which changes the sum of the repulsive force. Also, it suffers from a collision at point B by ignoring the repulsive force against a small obstacle such as a human compared with a large obstacle such as a wide wall. The simulation results show that with the PFM, the repulsive force of a small obstacle can be over-looked by that of a large obstacle. However, there does not exist any oscillation or collision in case (b), which is the result of the new obstacle avoidance.

4.2 Experimentation

The operator at the local site can control the robot at the remote site by using the client program over the Internet, as shown in Figure 15.

The operator generally recognizes the remote environment with the vision data. However, he cannot recognize under certain circumstances his view of the remote environment is limited on account of the narrow view-angle of the camera, the limitation of communication bandwidth, and

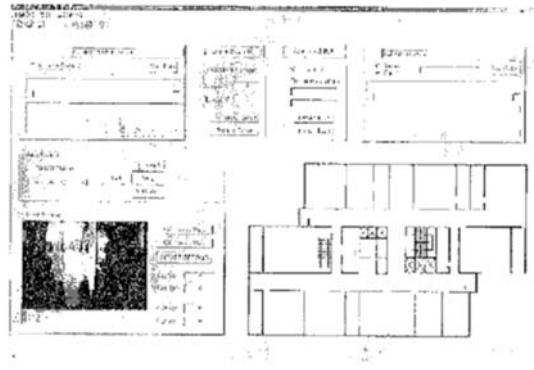

Fig. 15 User interface for tele-operated mobile robot over the Internet

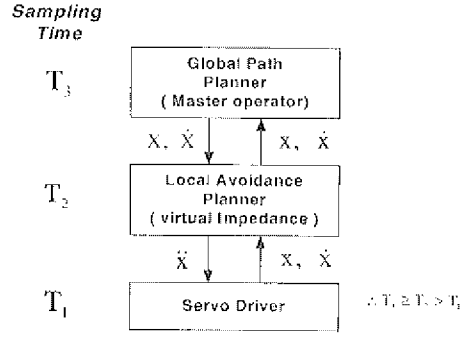

Fig. 16 Sampling time and the control structure of tele-operation system

the lack of lighting. The sampling time for the GPP, T_3, is set to be greater than or equal to the sampling time of the DAP, T_2=250 [ms]. And the sampling time for the servo driver is T_1=50 [ms] as shown in Figure 16. In this study, time delay problem such as the transmission delay of a velocity and position command in the Internet environment, is not considered. When a human operator controls the joystick, the motion command is generated. And it is transferred to the remote slave robot every 250 ms according to the direction of joystick displacement through the Internet. Therefore, the velocity of mobile robot is limited to 15 cm/sec.

Figure 17(a)-(f) is the experimental results, captured picture, of obstacle avoidance for mobile robot according to force-reflective joystick control. The virtual force from a mobile robot, which is a new function of the collision vector from 16

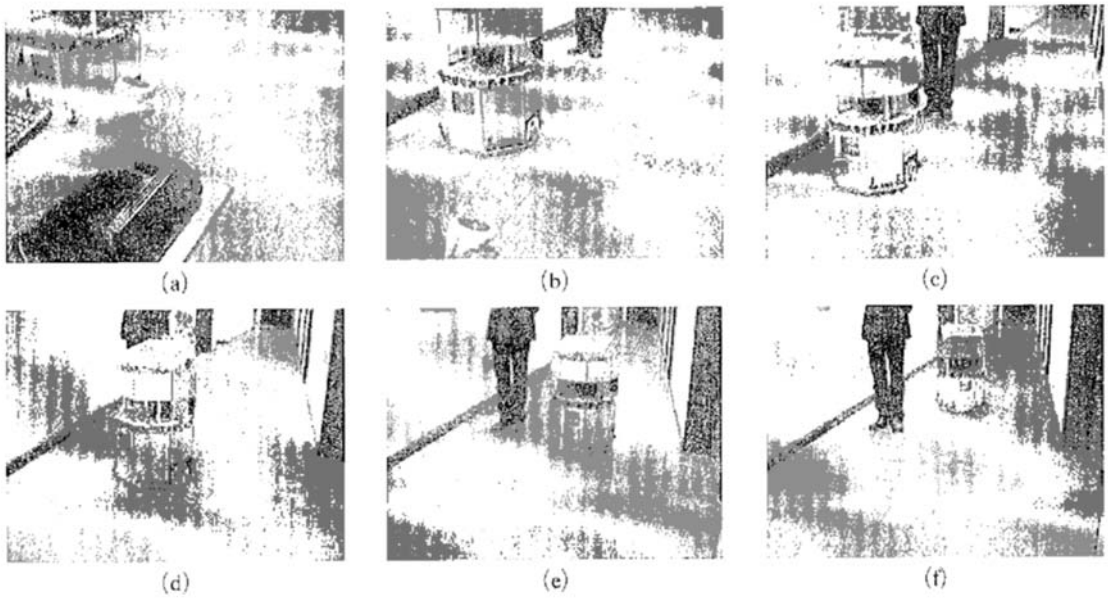

Fig. 17 Experimental result of obstacle avoidance for mobile robot

ultrasonic sensors, is reflected to the joystick as a force between the joystick and the human hand using two motors in the joystick. The two axial motors are driven by PWM outputs in proportion to the distance detected from collision vector. When a human operator controls the joystick to the direction of near obstacle, he can feel the virtual force in proportion to the distance and then control the joystick to the direction of free obstacles.

The new virtual impedance method is applied to the mobile robot tracking of a given path which avoids obstacles in real time. To validate the effectiveness of force-reflection in the tele-operation of a mobile robot, experiments are performed. In this experiment, the position and velocity of mobile robot are calculated using each encoder data of wheel and gyro sensor data at each control period and also the virtual force is calculated using sixteen ultrasonic sensors. Figure 18(a) and (b) are obtained as a result of the experimental data. Figure 18 (a) represents both situation in which the only vision information is reflected to the operator, and the vision and force information are delivered to the operator. Figure 18(b) represents the experimental result when the system combines autonomous obstacle avoidance

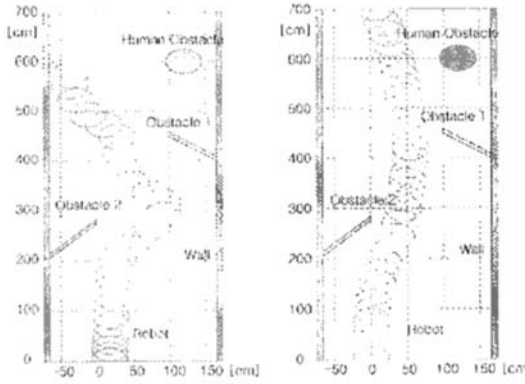

(a) Without a virtual force feedback

(b) With a virtual force feedback and autonomous obstacle avoidance

Fig. 18 Experimental results (where $K_r=2$, $D_r=10$, $K_o=4$, $D_o=10$, $M_s=10$)

with the vision and force information is delivered to the operator. At the time, the camera is fixed in the forward proceeding direction of the mobile robot. As shown by the experimental result in Figure 18(a), a human tele-operator must exercise extreme care to avoid obstacles in case of using only limited vision information, especially in obstacle-cluttered environments. Consequent-

ly, the actual traveling speed of the mobile robot might be very slow. In case of using both vision and force information, a human tele-operator can feel, and avoid, collisions through the joystick in spite of the limitations in visual display, but the mobile robot rocked from side to side, because it is very difficult to examine the actual distance between mobile robot and obstacles through one camera information. The system of autonomous obstacle avoidance with force-reflection can provide an ability of assuming the position and distance of obstacles from the mobile robot in spite of the limitations in visual display. The mobile robot follows the general direction prescribed by the operator. When the robot encounters an obstacle, it autonomously avoids collision with that obstacle, trying to match the operator's prescribed direction as close as possible.

As shown by the comparison of Figure 18(a) and (b), the latter situation is much safer than the former situation for obstacle avoidance. Although the success of obstacle avoidance is affected by the handling ability of the operator, we obtained similar results in the experiments for three different operators. Figure 19 shows the experimental data obtained for the tele-operation of Figure 18 (b). The first row represents the displacement of the joystick X_m, the second row shows the actual velocities in both directions of a mobile robot, and the last row displays the virtual force feedback to the operator.

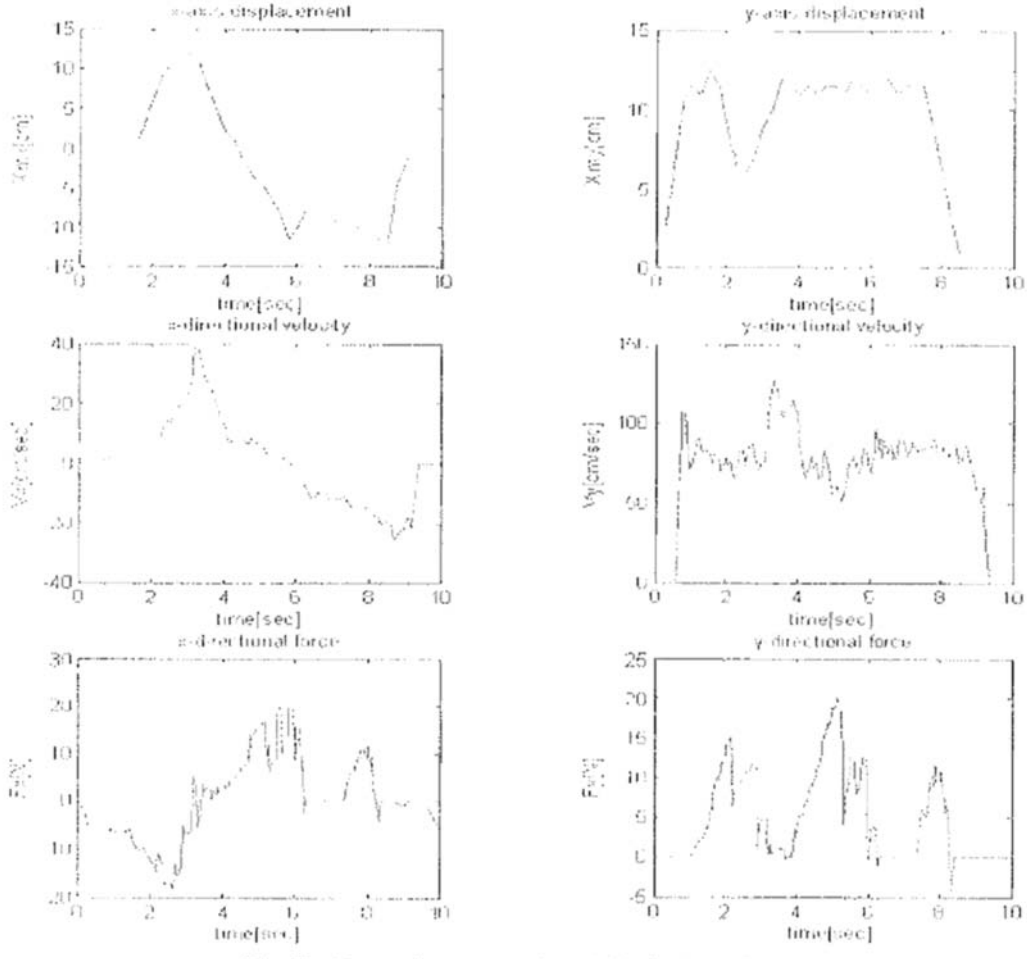

Fig. 19 Master site commands and the feedback force

5. Conclusions

A new virtual impedance method that enables a tele-operated mobile robot to follow the desired trajectory while avoiding obstacles in real-time, is proposed. In the proposed virtual impedance method, which utilizes a collision vector for obstacle avoidance, the virtual force is generated according to both the distance and the approach velocity between obstacles and the robot. This virtual force is reflected to the operator who holds the joystick that converts the force data to the corresponding physical quantities.

The autonomous obstacle avoidance with force-reflective system was implemented and tested successfully on an experimental system. It is shown experimentally that the operator can estimate the position of an obstacle in the remote environment by the virtual force regenerated from the force reflection joystick. That is, in spite of the limited visual information, the operator can feel the spatial sense against the remote environment by using the proposed method. When the robot encounters an obstacle, it autonomously avoids collision with that obstacle, trying to match the operator's prescribed direction as close as possible. Therefore, the tele-operated mobile robot can perform highly skillful tasks in the unstructured environment with an operator who monitors and moves a joystick to generate intelligent commands.

References

Arai, T., Ogata, H. and Suzuki, T., 1989, "Collision Avoidance among Multiple Robots Using Virtual Impedance," *Proc. of IEEE/RSJ Int. Workshop on Intelligent Robots and Systems*, pp. 479~485.

Borenstein, J. and Koren, Y., 1988, "Obstacle Avoidance with Ultrasonic Sensors," *IEEE J. of Robotics and Automation*, Vol. RA-4, No. 2, pp. 213~218.

Borenstein, J. and Koren, Y., 1989, "Real-time Obstacle Avoidance for Fast Mobile Robots," *IEEE Trans. on System, Man and Cybernetics*, Vol. 19, No. 5, pp. 1179~1187.

Borenstein, J. and Koren, Y., 1990, "Teleautonomous Guidance for Mobile Robots," *IEEE Trans. on System, Man and Cybernetics*, Vol. 20, No. 6, pp. 1437~1443.

Elfes, A., 1987, "Sonar-Based Real-World Mapping and Navigation," *IEEE J. Robotics Automation*, Vol. RA-3, No. 3, pp. 249~265.

Elhajj, I., Xi, N., Fung, W. K., Liu, Y. H., Li, W. J., Kaga, T. and Fukuda, T., 2001, "Haptic Information in Internet-Based Teleoperation," *IEEE/ASME Trans. on Mechatronics*, Vol. 6, No. 3, pp. 295~304.

Hogan, N., 1985, "Impedance Control: An Approach to Manipulation Part I-III," *Transactions of ASME-Journal of Dynamic Systems*, Measurement, and Control, Vol. 107, No. 3, pp. 1~24.

Khatib, O., 1986, "Real Time Obstacle Avoidance for Manipulators and Mobile Robots," *International Journal of Robotics Research*, Vol. 5, No. 1, pp. 90~96.

Kim, W., Hannaford, B. and Bejczy, A., 1992, "Force-Reflection and Shared Compliant Control in Operating Telemanipulators with Time Delay," *IEEE Trans. on Robotics and Automation*, Vol. 8, No. 2, pp. 176~185.

Lawrence, D. A., 1993, "Stability and Transparency in Bilateral Teleoperation," *IEEE Trans. on Robotics and Automation*, Vol. 9, No. 5, pp. 624~637.

Lee, S. S. and Lee, J. M., 2000, "Haptic Interface Design for the Tele-Surgery," *Proc. of the CIDAM Workshop on Service Automation and Robotics*, Hong Kong, pp. 81~91.

Ota, J., Arai, T., Yoshida, E., Kurabayashi, D. and Mori, T., 1995, "Real Time Planning Method for Multiple Mobile Robots," *Proc. of IEEE Int. Symposium on*, Assembly and Task Planning, pp. 406~411.

Roh, D. K., Kim, I. M., Kim, B. H. and Lee, J. M., 2001, "Localization of a Mobile Robot Using the Information of a Moving Object," *J. of Control, Automation and Systems Engineering*, Vol. 7, No. 11, pp. 933~938.

Zhao, Y. and BeMent, S. L., 1992, "Kinematics, Dynamics and Control of Wheeled Mobile Robots," *Proc. of IEEE Conf. Robotics and automation*, pp. 91~96.